Chinese Chemical Letters 37 (2026) 111631

Contents lists available at ScienceDirect

Chinese Chemical Letters

journal homepage: www.elsevier.com/locate/cclet

Microwave assisted metal-free catalysts preparation from waste plastics for efficient pollutants degradation: Interesting relationship between plastic types and nonradical/radical pathways

Denghong Zhao[a], Mingwei Yang[a], Yichuan Zhang[a], Long Qin[a], Hang Liu[a], Hongji Chen[a], Maoguo Tan[a], Zhongyi Yin[a], Bin Sun[a], Yu Shen[a], Haijiao Xie[b], Heyan Jiang[a,*]

[a] Key Laboratory of Catalysis Science and Technology of Chongqing Education Commission, Chongqing Key Laboratory of Environmental Catalysis, Chongqing Technology and Business University, Chongqing 400067, China
[b] Hangzhou Yanqu Information Technology Co., Ltd., Hangzhou 310003, China

ARTICLE INFO

Article history:
Received 22 February 2025
Revised 6 June 2025
Accepted 22 July 2025
Available online 25 July 2025

Keywords:
Waste plastic
Porous carbon material
Microwave pyrolysis
Peroxymonosulfate
Nonradical/radical pathways

ABSTRACT

To implement the principle of utilizing waste to address waste issues, porous carbon catalytic materials, prepared through a straightforward process involving NaOH-assisted microwave pyrolysis of ubiquitous waste plastics, were employed to degrade pollutants *via* peroxymonosulfate (PMS) activation. Polyethylene terephthalate (PET) derived P_1S_2 exhibited characteristics of defects enrichment and C=O formation, while H_1S_2, prepared by carbonization of high-density polyethylene (HDPE), possessed a large number of C–OH and defects. Metal-free catalysts P_1S_2 and H_1S_2 exhibited excellent tetracycline (TC) degradation performance, with the rate constants up to 0.303 min^{-1} and 0.235 min^{-1}. Interestingly, mechanism studies demonstrated that the types of waste plastic precursor had a significant impact on the pathways involved in TC degradation. Specifically, carbon defects in P_1S_2 dominated the electron transfer nonradial degradation pathway of TC; However, C–OH in H_1S_2 served as the reactive site for main active species $SO_4^{\bullet-}$/$^{\bullet}$OH generation, initiating a free radical pathway. In addition, by combining Fukui function calculation and LC-MS test during the TC degradation process, the vulnerable sites attacked by active species were identified; different degradation routes of TC in nonradial and radial pathways were proposed and discussed. Furthermore, the toxicity of all intermediates was analyzed using the toxicity assessment software. This study offers fresh insights into the critical role of carbocatalysts derived from various waste plastics in both nonradical and radical activation processes of PMS.

© 2025 Published by Elsevier B.V. on behalf of Chinese Chemical Society and Institute of Materia Medica, Chinese Academy of Medical Sciences.

The extensive application of antibiotics across diverse sectors, encompassing animal husbandry, agriculture as well as medical practice, has resulted in the appearance of antibiotic resistant genes as well as antibiotic resistant bacteria in natural environment [1]. Due to their harmful impacts on both human health and ecosystem, World Health Organization has categorized them as a significant public health threat in 21st century [2]. Tetracycline (TC) is a broadly utilized antibiotic in both medical practice and animal farming. Its potent antibacterial properties, coupled with notable ecological toxicity, potential carcinogenic effects, and resistance to natural biodegradation, render even minute concentration of TC in the environment an obvious threat to human [3]. Consequently, there is an immediate need for an efficacious strategy to manage TC, thereby mitigating associated environmental risks. Peroxymonosulfate (PMS)-involved advanced oxidation processes (AOPs) have demonstrated notable efficacy for recalcitrant organic pollutants removal, attributed to the high oxidative potential of reactive oxygen species (ROS), rapid reaction kinetics, and their applicability in a broad pH range [4]. For instance, Hu *et al.* [5] successfully prepared a bubble network catalyst, Co@NCNTs-*T* ($T = 500$, 600, 700 °C), through a simple one-step calcination method. These catalysts were constructed by encapsulating small cobalt nanoparticles within N-doped carbon nanotubes and sewing them into a bubble-like structure. This unique design significantly enhanced the inactivation resistance during the degradation of TC through PMS activation. Conventional metal-based catalytic materials are extensively used to activate PMS. Nevertheless, the majority of metal catalysts unavoidably suffer from the drawback of secondary pollution, stemming from the leaching of metal ions [6].

Up to now, carbon materials have demonstrated extensive accessibility, ecological compatibility, along with straightforward

* Corresponding author.
E-mail address: orgjiang@163.com (H. Jiang).

https://doi.org/10.1016/j.cclet.2025.111631
1001-8417/© 2025 Published by Elsevier B.V. on behalf of Chinese Chemical Society and Institute of Materia Medica, Chinese Academy of Medical Sciences.

preparation techniques. Owing to their non-metallic composition, excellent stability, as well as abundance of active sites, they are regarded as promising green catalysts and have found widespread application in effluent treatment [6–8]. The catalytic performance of carbon materials is contingent upon their structural configuration, functional moieties, defects, as well as inherent properties [9]. Usually, the advanced oxidation degradation of pollutants by non-metallic carbon materials can be dominated by both nonradical and free radical pathways [10]. In nonradical way, the degradation of pollutants can mainly be achieved through electron transfer. It is proposed that defective regions within carbon materials are reactive sites for activating PMS, leading to the formation of reactive complexes for nonradical degradation. This robust interplay between defects and contaminants enables PMS to degrade target compounds efficiently through the extraction of electrons from adsorbed substances, thereby bypassing the formation of free radicals [11]. Wang *et al.* [12] prepared ionic liquids (IL) derived porous C material as PMS activators for the naproxen oxidation and degradation. They demonstrated that abundant defect sites on the porous carbon material N-PC1000 served as active sites facilitating direct electron transfer. These sites were capable of restricting delocalized π system with a "localized state", thus exhibiting distinctly different chemical as well as electronic characteristics. They also confirmed that the efficiency of organic matter removal increased as the defect level of porous carbon materials rose. On the other hand, in the radical pathway, the introduction of N (such as graphic N and pyrrolic N) or C–OH in the material may affect persulfate activation and produce different active species [13–15]. For example, the graphitic N enriched metal-free N-rGO prepared by Kang *et al.* [13] exhibited efficient capability in activating persulfate to generate reactive species, thereby facilitating sulfachloropyridazine removal, while pyrrolic N possessed relatively lower thermal stability and was prone to conversion to graphitic nitrogen. Moreover, graphitic N possesses greater electronegativity along with smaller atom radius, which facilitates electron transfer from adjacent carbon atoms, thereby enhancing charge density of neighboring carbon [16]. In such instances, radical way prevails over electron transfer approach. Owing to their chemical inertia, pristine carbon typically displays limited reactivity in activating PMS [17]. As a consequence, formulating more appropriate modification strategies to augment the catalytic degradation efficacy of non-metallic carbon materials continues to pose significant challenges.

Plastics, particularly those that are naturally non-degradable like polyethylene terephthalate (PET), polyethylene (PE), as well as polypropylene (PP), are widely utilized in the packaging, construction, along with textile sectors due to their value and malleability [18]. Thousands tons of waste plastics exacerbate new environmental challenges and represent a considerable depletion of resources [19]. In light of this, significant endeavors are undertaken to repurpose plastics and enhance their conversion to higher-value products. Plastics are carbon rich materials, so converting waste plastics into carbon materials including graphene, carbon nanosheets, and porous carbon is currently one of the research hotspots [20,21]. These carbon materials obtained from plastics exhibit versatility in their applications, encompassing supercapacitors, batteries or separation processes [18,22], as well as water purification techniques [23,24]. Currently, the primary methods for converting waste plastics into carbon involve traditional pyrolysis techniques. However, microwave treatment has demonstrated superiority over traditional pyrolysis in aspects such as energy transfer efficiency, enhanced yield of material, and its capability for instant and precise temporal control [25–27]. Zhou *et al.* [26] employed cobalt nitrate as a microwave adsorber to prepare carbon material catalyst $S_{0.3}$-Co@P_2C, which exhibited obvious porous properties, through microwave pyrolysis of waste plastic PET. Within just 15 min, thoroughly carbamazepine removal was accomplished using $S_{0.3}$-Co@P_2C. The research introduces an innovative method for waste plastics application *via* microwave carbonization. However, due to the composition of non-polar molecules in plastics, they basically do not absorb or absorb very little microwave radiation. So far, the use of microwave treatment for metal-free carbonization of waste plastics is still quite limited.

Thereby in this study, for the first time, common waste plastics PET and high-density polyethylene (HDPE) were selected as carbon sources to fabricate metal-free porous carbon materials through a simple microwave pyrolysis method, with sodium hydroxide as microwave absorber along with pore-forming agent and sodium lignosulfonate as carbonization auxiliary. The P_1S_2 material derived from PET exhibited characteristics indicative of defect enrichment along with the formation of C=O bonds. In contrast, H_1S_2, which was prepared through the carbonization of HDPE, possessed a significant quantity of C–OH groups and defects. Waste plastics derived P_1S_2 and H_1S_2 demonstrated remarkable efficiency in degrading TC, with degradation rate constants as high as 0.303 min^{-1} and 0.235 min^{-1}. In addition, influence of catalyst dose, PMS amount, TC concentration, pH, temperature, and anions on TC removal were also checked. By employing correlation fitting, quenching experiments, and electron paramagnetic resonance (EPR) analysis, TC degradation was predominantly facilitated by electron transfer in P_1S_2/PMS system, where defects served as the primary active sites. In the meantime, removal of TC in the H_1S_2/PMS was predominantly facilitated by free radicals governed pathway, with C–OH serving as the primary active sites. The removal mechanism of TC was deduced by utilizing the Fukui function calculation, which pinpointed the susceptible sites for attack by active species, along with the identification of reaction intermediates through LC-MS.

The preparation method of carbon materials was demonstrated in Fig. 1a. Typically, 0.5 g waste PET powder, 1.0 g sodium lignosulfonate, and 0.5 g sodium hydroxide were well grinded in ceramic mortar. Mixture was placed in a 25 mL crucible and pyrolyzed at 800 W for 5 min (Table S1 was the selection criteria for preparation conditions). Due to the inability to directly carbonize waste plastic powder by microwave treatment in the presence of sodium hydroxide, biomass lignosulfonate sodium was used to assist in the waste plastics carbonization, while sodium hydroxide was used as both a microwave absorber and a pore-forming agent in the carbon materials formation. The resulting material was washed with H_2O/EtOH 5 times. After vacuum drying at 60 °C for 12 h, P_1S_2 was obtained. Keeping the weight amount of sodium hydroxide at 0.5 g and the total mass of PET powder and sodium lignosulfonate at 1.5 g, when the weight ratios of PET powder to sodium lignosulfonate were 1:4, 1:3, 1:2 and 1:1, the prepared materials were named as P_1S_4, P_1S_3, P_1S_2 and P_1S_1, respectively. When PET powder was replaced by HDPE powder, H_1S_2 was prepared under the same conditions as P_1S_2. C was prepared by microwave pyrolysis of 1.5 g sodium lignosulfonate, 0.5 g sodium hydroxide under 800 W conditions for 5 min without waste plastic. For comparison, P_1S_2–600 and H_1S_2–600 were also prepared by carbonizing at 600 °C for 2 h under N_2.

The appearance alongside pore features of carbon materials were examined utilizing scanning electron microscopy (SEM) and transmission electron microscopy (TEM) in Figs. 1b-g [28]. The non-metallic porous carbon catalysts P_1S_2 and H_1S_2 derived from waste plastics PET and HDPE exhibited significant porous structural characteristics. The formation of porous structures was not only attributed to the gases emitted during the pyrolysis of plastics and sodium lignosulfonate [29,30], which facilitated the pore formation, but also ascribed to the fact that NaOH, the activation reagent encapsulated in plastics-derived carbon material, was washed out to produce porosity. TEM element mapping (Figs. 1d

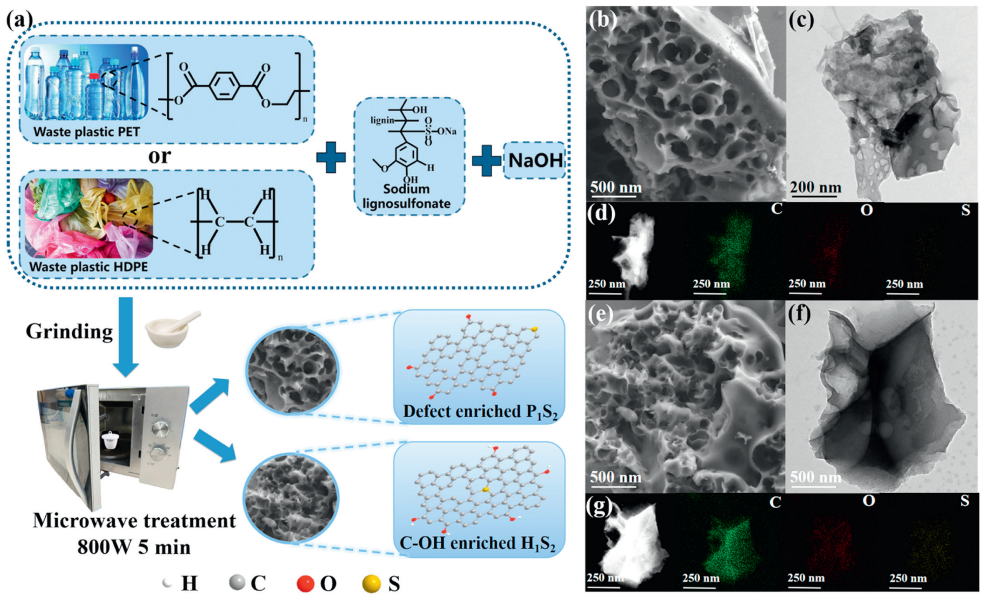


Fig. 1. (a) Schematic synthesis of carbocatalysts P_1S_2 and H_1S_2. (b-d) SEM, TEM along with TEM elemental mapping of P_1S_2. (e-g) SEM, TEM along with TEM elemental mapping of H_1S_2.

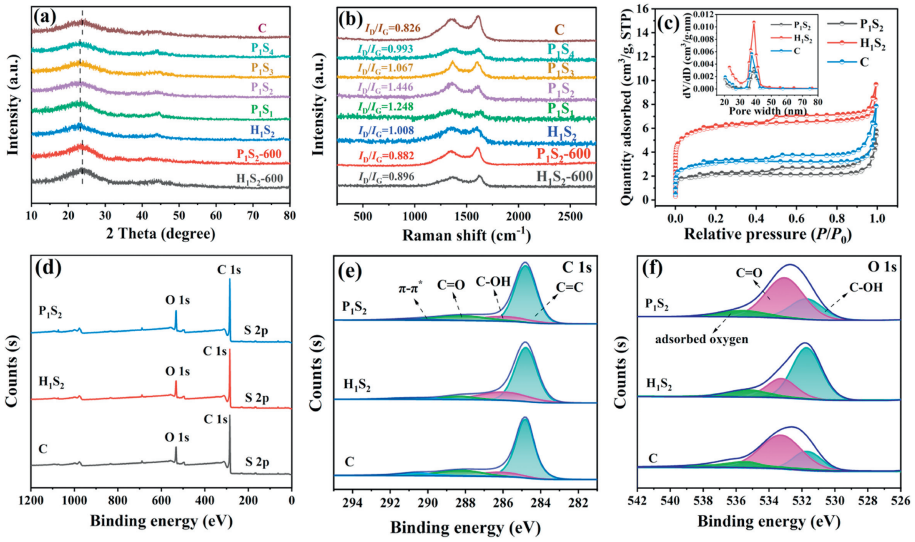


Fig. 2. (a) XRD patterns and (b) Raman spectroscopy of C, P_1S_4, P_1S_3, P_1S_2, P_1S_1, H_1S_2, P_1S_2–600 and H_1S_2–600. (c) Nitrogen adsorption desorption curves of P_1S_2, H_1S_2 and C (Inset: pore size distribution). The XPS survey (d), high resolution XPS for C 1s (e) and O 1s (f).

and g) showed well distribution of C, O, and S in P_1S_2 and H_1S_2 [26].

Crystal structure of prepared carbon material was inspected using X-ray diffraction (XRD) (Fig. 2a). No peak of waste plastic was detected in all samples, indicating completely carbonization of plastics (Fig. S1 in Supporting information). All as-prepared catalysts exhibited two broad signals around 23.1°–24.0° and 44.1°, ascribing to (002) along with (100) planes of amorphous carbon and crystalline carbon [15]. In contrast to the C without adding plastic, the (002) diffraction peak of amorphous carbon widened and shifted from 23.12° to 24.0° after adding PET. The broadening and displacement of diffraction (002) peak suggested defects along with amorphous carbon structures in catalytic materials [31]. Moreover, compared with traditional pyrolysis method, the (002) diffraction peak in carbon materials prepared by microwave was significantly broadened, implying that microwave treatment was also helpful for the generation of defects and amorphous structure. Further replacing PET with waste plastic HDPE (weight ratio of 2:1 between plastic and sodium lignosulfonate), the carbon material produced *via* microwave treatment also exhibited characteristic of defects and amorphous carbon structures. In Raman spectroscopy, D band around 1350 cm^{-1} as well as G band around 1580 cm^{-1} represent disordered carbon along with graphitized carbon [32]. I_D/I_G is generally applied to quantify defects level in catalysts. With the increase of PET plastic content, the defects of C, P_1S_4, P_1S_3, and P_1S_2 gradually increased (Fig. 2b), and the I_D/I_G value of P_1S_2 reached 1.446. The formation of porous structure in P_1S_2 might be the reason for the increase in defect degree. As PET further increased, the I_D/I_G value of P_1S_1 reduced, which may be due to excessive PET being unfavorable for defect formation. In HDPE derived carbon materials, the I_D/I_G value was 1.008, and the defect degree was equivalent to the graphitization degree, indicating that there may be differences in the mechanism of P_1S_2 and H_1S_2 during PMS activation for pollutant degradation. Compared

with the microwave carbonized materials P_1S_2 and H_1S_2, the decrease in I_D/I_G values of P_1S_2–600 and H_1S_2–600 indicated that microwave was more conducive to the formation of defect carbon than the traditional pyrolysis method. In addition, EPR test further showed that the content of vacancy defects in P_1S_2 was more obvious than that in H_1S_2 (Fig. S2 in Supporting information) [33,34]. Nitrogen adsorption desorption isotherms were investigated to exam specific surface area (SSA) and pore characteristics. The isotherms of catalysts exhibited conformity with type IV isotherms. H3 hysteresis loop within the range of 0.45 to 0.98 P/P_0 was indicative of mesoporous structure (Fig. 2c) [35]. In comparison with waste plastics-free C (SSA: 130.84 m^2/g), the SSA of H_1S_2 increased prominently to 264.57 m^2/g; while, the SSA of P_1S_2 slightly decreased to 91.83 m^2/g. However, when the traditional pyrolysis method was used, the SSA of P_1S_2–600 (34.64 m^2/g) and H_1S_2–600 (38.27 m^2/g) dramatically decreased (Fig. S3 in Supporting information). These results were explained that, compared to microwave calcination, tube furnace calcination was detrimental to increasing the SSA of carbon materials. Components along with valence states of catalysts were checked with X-ray photoelectron spectroscopy (XPS) (Tables S2-S5 in Supporting information) [36]. Fig. 2d, Figs. S5a and S6a (Supporting information) showed the full scan of P_1S_2, H_1S_2, C, P_1S_2–600 and H_1S_2–600, in which C, O and S were clearly visible. In order to study valence states of C, O as well as S, high-resolution XPS was utilized. The C 1s near 284.8, 286.2, 288.4, 290.8 eV were C=C, C–OH, C=O, π-π^* (Fig. 2e) [16,37]. The C=O content in P_1S_2 exceeded that of H_1S_2 and C, while C–OH content in H_1S_2 was significantly greater than P_1S_2 and C. As C=O and C–OH were widely recognized as active sites for activating PMS to degrade pollutants [14,15,38], different types of waste plastic may modulate contaminants removal pathway through affecting the exposure of different active sites in carbon materials. C=O peak in traditional pyrolysis prepared P_1S_2–600 was lower than that in microwave-assisted P_1S_2, and the C–OH peak in H_1S_2–600 was also lower than that in microwave-assisted H_1S_2, indicating that traditional pyrolysis was not favorable for C=O and C–OH generation (Figs. S5b and S6b in Supporting information). O 1s around 531.7, 533.2, and 535.4 eV (Fig. 2f) were C–OH, C=O, and adsorbed oxygen. Similarly, characteristic peak of C=O in P_1S_2 was significantly higher than that in H_1S_2, and feature peak of C–OH in H_1S_2 was the most prominent, which were corresponded to the phenomenon observed in the C 1s spectrum. Compared with H_1S_2 and C, some C=O group in P_1S_2 should mainly directly came from PET. For S 2p spectra in the catalytic materials (Fig. S4, Figs. S5d and S6d in Supporting information), signals around 164.0 and 165.0 eV were attributed to thiophene S $2p_{3/2}$ and $2p_{1/2}$ [39]. Meanwhile, 168.5 and 169.7 eV was attributed to surface bound sulfites and sulfates. The S 2p spectrum indicated the presence of various states of sulfur in all materials. Elemental analysis of various carbon materials could be found in Table S6 (Supporting information). The combined results of XPS and elemental analysis indicated that the prepared carbon materials were organic carbon materials.

The TC removal efficiency over different materials was analyzed in Figs. 3a and b and Fig. S7 (Supporting information). As the low kinetic constant of PMS self-oxidation ($k_{obs} = 0.018\ min^{-1}$), TC degradation of pure PMS was only 17.4%. Degradation ability of C/PMS towards pollutant was also very low, with TC degradation of only 67.8% within 20 min, suggesting that PMS activating ability over C alone without adding waste plastics was very limited. It could be evidently seen that, compared with P_1S_2–600/PMS (72.2%), the degradation performance of P_1S_2/PMS system (100%) was significantly improved, accompanied by a substantial increase in rate constant from 0.114 min^{-1} to 0.303 min^{-1}. Excellent TC removal performance of P_1S_2 should be attributed to the use of PET plastic as well as the application of microwave. These factors facilitated the generation of C=O active sites and defects for PMS activation improvement along with charge transfer enhancement. These, in turn, might trigger a nonradical degradation pathway [6]. Further investigation was conducted on the effect of PET to sodium lignosulfonate mass ratio during the P_1S_2 preparation on the TC removal efficiency. Catalytic performance showed an upward trend at the beginning followed by a decline as plastic content gradually rose (Fig. 3b). The rate constants of P_1S_4, P_1S_3, P_1S_2, and P_1S_1 were 0.098, 0.125, 0.139, 0.303, and 0.159 min^{-1}, suggesting that P_1S_2 had the highest TC degradation efficiency (effect under different conditions on TC removal see Fig. S10 in Supporting information). After determining the optimal ratio of 1:2 between plastic and sodium lignosulfonate, further exploration was conducted to prepare H_1S_2 using HDPE instead of PET, and the degradation performance of HDPE derived carbon materials on TC was studied (Fig. 3a, Fig. S7a). As shown in Fig. 3a, the degradation performance of H_1S_2/PMS system (100%, $k_{obs} = 0.235\ min^{-1}$) was significantly higher than that of H_1S_2–600/PMS (78.4%, $k_{obs} = 0.135\ min^{-1}$). The remarkable degradation capabilities of H_1S_2 could be related to the use of HDPE plastic as well as microwave, which were more beneficial to C–OH active site generation for the free radical degradation pathway. The results of Figs. 3a and b showed that both waste plastics utilization and microwave pyrolysis were instrumental in improving pollutant degradation performance of carbon catalysts *via* active centers exposure. Table S7 showed the quantitative data on the advantages of microwave pyrolysis compared to traditional pyrolysis. Considering that the high specific surface area of carbon materials may adsorb TC, adsorption tests were carried out to elucidate the role of catalytic processes in TC removal (Fig. S8 in Supporting information). The experimental results displayed that TC adsorption capacities of C, P_1S_2, P_1S_2–600, H_1S_2, and H_1S_2–600 were 30.9%, 27.2%, 24.6%, 22.0%, and 27.2%, respectively. In contrast, the direct TC removal process exhibited a similar speed compared to the process involving a 20 min pre-adsorption step (Fig. S9 in Supporting information). Consequently, the TC removal process described here predominantly relies on catalysis rather than adsorption. Further cycling experiments, mineralization tests, and substrate expansion experiments collectively demonstrated the outstanding stability of catalysts, effective mineralization of TC, and universality (Figs. S10 and S11 in Supporting information).

To elucidate the main active sites in P_1S_2/PMS and H_1S_2/PMS catalytic systems, correlation fitting between possible active sites and degradation efficiency was performed in two systems (Figs. 3c-f). From Raman and XPS, it was not difficult to see that P_1S_2 prepared by microwave carbonization had obvious carbon defects and substantial C=O group. Therefore, linear fitting was performed to investigate the relationship between the carbon defects or C=O content in specific materials (including C, P_1S_2–600, P_1S_2) and the TC removal rate as well as the degradation kinetics constant within catalytic systems. The removal rate and k_{obs} of TC demonstrated a linear relationship with the increase of defects number (Fig. 3c), showing a good correlation, with correlation coefficients as high as 0.996 and 0.999, respectively. In contrast, the correlation between C=O content and TC removal rate along with k_{obs} was not high (Fig. 3d). Although it was widely reported in literature that C=O was the main active site for generating $^1O_2$, considering the low oxidation ability and poor stability of $^1O_2$, its ability in pollutant removal may be overestimated [40]. Therefore, electron transfer caused by defects should be the main process of pollutant degradation over P_1S_2/PMS, while C=O site induced $^1O_2$ should play a minor role. On the other hand, Raman and XPS indicated that the most prominent feature of H_1S_2 material prepared by microwave carbonization of HDPE was its abundant hydroxyl functional groups and some carbon defects. Therefore, linear fitting was performed on the C–OH content and defects in C, H_1S_2–600, and H_1S_2 based on the degradation experiment results. The correlation between C–OH content and TC removal rate along with k_{obs} was

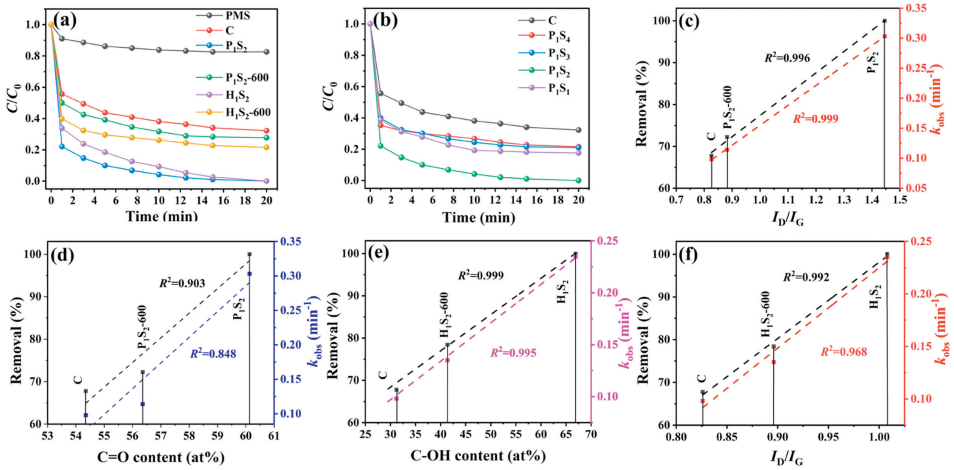


Fig. 3. (a, b) TC degradation over various materials. Correlation of TC removal ratio along with k_{obs} to I_D/I_G (c) and C=O content (d) over C, P_1S_2–600 and P_1S_2. Correlation of TC removal ratio along with k_{obs} to C–OH content (e) and I_D/I_G (f) over C, H_1S_2–600 and H_1S_2. Reaction conditions were $[TC]_0$: 10 mg/L, [PMS]: 0.6 g/L, [catalyst]: 0.10 g/L, pH: 6.8, *T*: 25 °C.

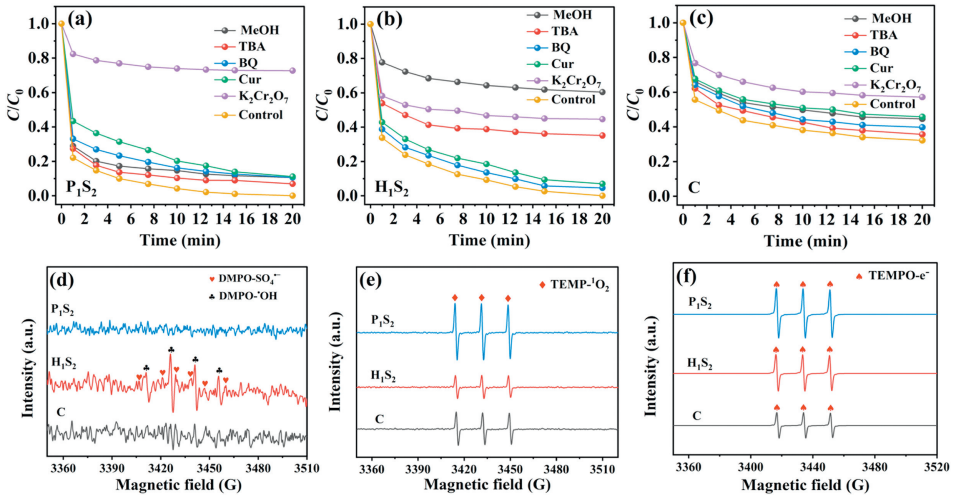


Fig. 4. Effect of different quenching agents on TC removal over P_1S_2/PMS (a), H_1S_2/PMS (b), and C/PMS (c) systems. EPR tests for •OH and $SO_4^{\bullet-}$ (d), $^1O_2$ (e) as well as e^- (f) of above systems. Reaction conditions were $[TC]_0$: 10 mg/L, [PMS]: 0.6 g/L, [catalyst]: 0.10 g/L, pH: 6.8, *T*: 25 °C.

pretty good (R^2 values: 0.999 and 0.995, Fig. 3e). According to relevant reports, C–OH could activate persulfate to form free radicals [14,15]. Therefore, free radical pathway should play an important role in activating PMS to degrade TC in HDPE derived carbon material H_1S_2. There was a certain correlation between defects amount and TC degradation efficiency (Fig. 3f), thus, the effect of defects induced charge transfer in TC removal should not be ignored.

To confirm the contribution of active species during degradation, TC removal was conducted in the presence of various scavengers. As illustrated in Fig. 4a, the presence of either 10 mmol/L MeOH (scavenger for $SO_4^{\bullet-}$ as well as •OH) or TBA (typical scavenger for detecting •OH) in P_1S_2/PMS exhibited no significant inhibition during TC removal with slightly decreased TC removal rate of 89.5 % and 93.1 % [26]. Consequently, it was confirmed that TC removal in the P_1S_2/PMS system did not rely on these two radicals. Moreover, *p*-benzoquinone (BQ) as well as curcumin (Cur) were utilized as scavengers of $O_2^{\bullet-}$ and singlet oxygen ($^1O_2$). The presence of BQ had no obvious inhibition with 89.4 % TC degradation, indicating that $O_2^{\bullet-}$ radicals had a rather limited role. After adding Cur, the inhibition of TC degradation was quite limited with a degradation efficiency of 88.8 %, which may be related to the low oxidation ability and poor stability of $^1O_2$. After adding e^- scavenger $K_2Cr_2O_7$, 72.7 % of TC degradation efficiency was suppressed, indicating that e^- played pretty important role in P_1S_2/PMS system [36]. In comparison, a similar rule was observed in the quenching experiment of P_1S_2–600/PMS system (Fig. S15a in Supporting information), and the relatively lower degradation efficiency in P_1S_2–600/PMS should be related to the lower defect content in P_1S_2–600, thereby hindering electron transfer from TC to PMS. Fig. 4b revealed an interesting finding that the H_1S_2/PMS system showed obviously different results in the quenching experiment compared to the P_1S_2/PMS system, that is, with MeOH or TBA, TC removal decreased sharply (the TC degradation rates only reached 40.0 % and 64.9 %, respectively), indicating that $SO_4^{\bullet-}$ and •OH had important contribution during TC removal. In combination with the XPS result, $SO_4^{\bullet-}$ and •OH should be generated through PMS activation by C–OH. On the other hand, electron quenching experiment showed that the electron transfer induced pollutant degradation in H_1S_2/PMS was clearly lower than in P_1S_2/PMS. Furthermore, BQ or Cur almost exhibited no inhibitory effect on TC removal in H_1S_2/PMS, indicating that $O_2^{\bullet-}$ and $^1O_2$ had rather limited contribution. Similarly, $SO_4^{\bullet-}$, •OH and electron transfer also played important roles in TC removal over H_1S_2–600/PMS system. Compared to the H_1S_2/PMS, the relatively lower degradation efficiency in the H_1S_2–600/PMS system should be attributed to the lower C–OH content and less defects in the H_1S_2–600 prepared

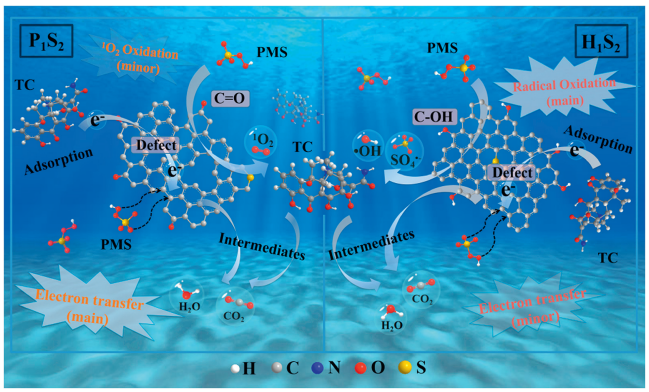


Fig. 5. The proposed mechanism of P_1S_2/PMS as well as H_1S_2/PMS on TC removal.

by traditional pyrolysis. Finally, in the absence of waste plastics as a carbon source, the degradation efficiency of TC by material C was significantly reduced, and the role of $SO_4^{\bullet-}$/$^{\bullet}OH$ and electron transfer in pollutant degradation was rather limited (Fig. 4c). Given that the majority of carbon-based catalysts typically demonstrate a nonradical pathway accompanied by a weak or virtually insignificant radical pathway [8,23], the interesting discovery of modulating pollutant degradation pathways by adjusting the types of waste plastics offered novel insights into the design of carbon-based catalysts.

To offer deeper insight into the role of ROS in PMS activation, EPR spectral analysis was performed. During EPR tests, specific spin trapping agents were utilized: 5,5-dimethyl-1-pyrroline-*n*-oxide (DMPO) for the detection of $SO_4^{\bullet-}$, $^{\bullet}OH$, $O_2^{\bullet-}$ radicals; 2,2,6,6-tetramethyl-4-piperidone (TEMP) for $^1O_2$ identification; and 2,2,6,6-tetramethylpiperidine-1-oxyl (TEMPO) for e^- [41]. As illustrated in Fig. 4d, relatively strong peaks of DMPO-$SO_4^{\bullet-}$ along with DMPO-$^{\bullet}OH$ were observed in H_1S_2/PMS after adding DMPO. In contrast, no signals indicative of DMPO-$SO_4^{\bullet-}$ as well as DMPO-$^{\bullet}OH$ were observed in C/PMS as well as P_1S_2/PMS systems. The result of DMPO trapping experiments was consistent with the MeOH and TBA quenching experiments. $O_2^{\bullet-}$ was captured by DMPO in the presence of methanol. No $O_2^{\bullet-}$ signal was detected in all catalytic systems, which contradicted the quenching experiment results (Figs. S15d and S16 in Supporting information). This contradiction may be due to the rapid conversion of $O_2^{\bullet-}$ intermediate to $^1O_2$ [42]. Further detection of $^1O_2$ in the catalytic system using TEMP revealed the presence of $^1O_2$ in all catalytic systems (Fig. 4e and Fig. S15e in Supporting information). In combination with the $^1O_2$ quenching experiment, the role of $^1O_2$ in TC degradation was rather limited because of the low oxidation ability and poor stability of $^1O_2$. As shown in Fig. 4f and Fig. S15f (Supporting information), TEMPO-e^- signals were detected in all catalytic systems, revealing that e^- was existed during TC removal process in these five systems. The order of TEMPO-e^- signal strength was P_1S_2 > H_1S_2 > P_1S_2–600 > H_1S_2–600 > C, aligning with the findings derived from electron quenching experiments. It was worth mentioning that the signal intensity of TEMPO-e^- in P_1S_2/PMS system was obviously stronger than in H_1S_2/PMS system, which corresponded to the transition from the electron transfer pathway in P_1S_2/PMS to the free radical process in H_1S_2/PMS. Moreover, electrochemical experiments further verified the electron transfer mechanism (Fig. S17 in Supporting information).

Based on the above discussions, the TC degradation mechanisms through radical and nonradical pathways, mediated through PMS activation with P_1S_2 and H_1S_2 catalysts, were proposed (Fig. 5 and Eqs. S3-S12 in Supporting information). The types of waste plastic had significant regulatory effect on the activation mechanism between electron transfer dominated nonradical process and $SO_4^{\bullet-}$/$^{\bullet}OH$ dominated radical pathway. In P_1S_2/PMS system, defects were the main active sites and electron transfer was the dominant process for TC removal. The TC degradation process could be inferred as follows: (1) Thanks to the electrostatic interaction and van der Waals force, PMS was adsorbed onto defects, leading to the formation of carbon activated peroxymonosulfate complex (C-$S_2O_8^{2-}$). Meanwhile, electron-rich TC exhibited a tendency to donate electrons to C-$S_2O_8^{2-}$, facilitating PMS decomposition along with pollutants removal (Eq. S3) [15,37]. Notably, structure defects acted as electron shuttle channels, promoting electron transfer from TC to PMS. (2) PMS activation driven by C=O was another nonradical route for TC removal. In this scenario, C=O rendered PMS activation and $^1O_2$ production (Eqs. S4-S7) [38]. In addition, electron-rich C=O groups could function as Lewis active sites, enabling electron transfer to produce $O_2^{\bullet-}$ or $^1O_2$ (Eqs. S8 and S9) [43]. However, in the H_1S_2/PMS system, free radicals dominated the degradation of TC. Wherein, C–OH activated PMS to generate $SO_4^{\bullet-}$/$^{\bullet}OH$ for TC degradation, while defects triggered nonradical process played an auxiliary role. In radical pathway, when PMS was interacted with the C–OH on the surface of H_1S_2, C–OH functioned as electron donors, facilitating PMS reduction. This reduction led to the generation of HO_2^-, SO_4^{2-}, along with C=O (Eq. S10) [14]. Following this, HO_2^- further interacted with $S_2O_8^{2-}$ to form $SO_4^{\bullet-}$ and $O_2^{\bullet-}$ (Eq. S11). Notably, $O_2^{\bullet-}$ was primarily considered a precursor of $^1O_2$ through self-recombination with H_2O, rather than directly oxidizing pollutants (Eq. S9). Additionally, $^{\bullet}OH$ was generated through the reaction between $SO_4^{\bullet-}$ and H_2O (Eq. S12) [44]. Based on quenching experiments, electrochemical analysis as well as EPR tests, it could be deduced that $SO_4^{\bullet-}$ and $^{\bullet}OH$ free radical pathway dominated the TC oxidation, whereas electron transfer had a lesser contribution. In combination with FTIR spectra of PMS, P_1S_2 + PMS and H_1S_2 + PMS in Fig. S18 (Supporting information), it was supposed that: upon interaction with P_1S_2, PMS could form chemical bonds with vacancy defects, resulting in a significant elongation of the O–O bond, which would facilitate the nonradical degradation of TC *via* electron transfer; meanwhile, when interacted with H_1S_2, PMS could react with the O on C–OH, leading to the abstraction of an H atom from the -OH groups and the subsequent formation of $SO_4^{\bullet-}$ and $^{\bullet}OH$ radicals, which facilitated the removal of TC.

Until now, studies have shown that P_1S_2/PMS and H_1S_2/PMS generate distinct reactive species during TC removal. Subsequent intermediates along with TC degradation paths analysis were conducted to elucidate how varying ROS exerted different influences on TC removal mechanisms. The DFT-calculated condensed Fukui function (detailed in Text S4 in Supporting information) was employed to identify reactive sites vulnerable to ROS attack to confirm the TC degradation process (Fig. 6a, Table S8 in Supporting information). Specifically, f^- signifies electrophilic reaction connected with nonradical oxidation, f^0 stands for radical attack and f^+relates to nucleophilic reaction [45]. An increased value of f^0, f^- or f^+ within an atom correlates with a greater likelihood of it serving as the attack site for corresponding species [46]. Electron transfer, serving as the primary removal pathway for electron-rich TC in P_1S_2/PMS, is viewed as a process involving electrophilic attack [47]. Similarly, as another electrophilic species, $^1O_2$ readily targets the electron-rich sites on TC [46]. Additionally, $SO_4^{\bullet-}$ and $^{\bullet}OH$ conduct free radical attack. The LUMO (lowest unoccupied molecular orbital) and HOMO (highest occupied molecular orbital), unveiled locations prone to electrophilic attack and radical attack (Figs. 6b and c). Typically, the HOMO readily undergoes electron loss, making it highly susceptible to attack by electrophilic species [48]. As exhibited in Fig. 6c, the HOMO distributions of TC aligned with the active sites derived from Fukui index calculations. The sites exhibiting larger Fukui values signify a greater propensity for reactivity. As expected, $SO_4^{\bullet-}$and $^{\bullet}OH$ exhibited a

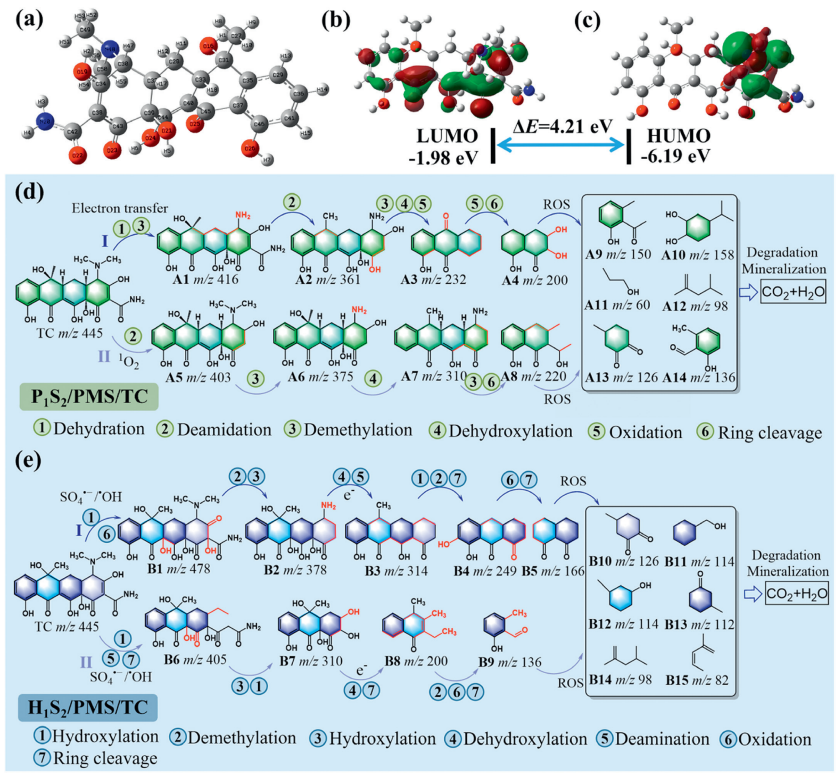


Fig. 6. Optimized TC structure (a). LUMO (b) and HOMO (c) of TC. The possible TC removal pathways over P_1S_2/PMS (d) and H_1S_2/PMS (e) systems.

propensity to target sites on benzene rings and oxygen-containing functionalities, whereas electron transfer processes and $^1O_2$ were more inclined to attack positions on nitride-containing groups. To quantify the reactivity of individual atoms within TC, the data presented in Table S8 (Supporting information) exhibited the natural population analysis (NPA) charge distribution, in conjunction with the Fukui index. In the P_1S_2/PMS/TC system, N48 ($f^-=0.68776$), O16 ($f^-=0.39696$), N20 ($f^-=0.3818$), C40 ($f^-=0.18607$), C27 ($f^-=0.30047$), C38 ($f^-=0.20305$), O21 ($f^-=0.38394$), O23 ($f^-=0.35539$), and O24 ($f^-=0.39606$) exhibited heightened reactivity and a propensity for electrophilic attack, aligning with the observations derived from HOMO as well as LUMO analyses. In the H_1S_2/PMS/TC system, C40 ($f^0=0.05519$), C38 ($f^0=0.03907$), N48 ($f^0=0.21846$), C29 ($f^0=0.01111$), C46 ($f^0=0.003715$), C41 ($f^0=0.00491$), C31 ($f^0=0.00145$), H51 ($f^0=0.0314$), O24 ($f^0=0.02882$), O19 ($f^0=0.00555$) characterized with higher f^0 values were more vulnerable to be attacked by $SO_4^{\bullet-}$/$^\bullet$OH radicals.

Additionally, to gain deeper insights into TC removal mechanism, LC-MS was utilized to identify the degradation intermediates (Fig. S19, and Tables S9 and S10 in Supporting information). Utilizing both the Fukui function and intermediates analysis, plausible TC removal pathways were deduced. Specifically, within P_1S_2/PMS/TC, two potential nonradical routes were presented (Fig. 6d) [8,49,50]. In the pathway I: **A1** (*m/z* 416) was generated *via* dehydrogenation subsequent to elimination of hydrogen atom at C32 and C33 through electron transfer, along with the removal of aminomethyl group on N48. **A1** then underwent further degradation to form **A2** (*m/z* 361) *via* processes of dehydration as well as deamidation. Additionally, continuous oxidation, dehydroxylation, demethylation and ring cleavage reaction yielded **A3** (*m/z* 232) and **A4** (*m/z* 200). In pathway II of the deamidation process, the N20 site on TC was attacked by $^1O_2$, resulting in the loss of amide group, and resulting in **A5** (*m/z* 403). Subsequently, **A5** lost *N*-methyl moiety on N48 site form **A6** (*m/z* 375) and simultaneously removed hydroxyl groups, conversing **A6** to **A7** (*m/z* 310). The subsequent demethylation and ring opening reaction formed **A8** (*m/z* 220). Ultimately, the intermediary small molecules were further broken down into **A9** (*m/z* 150), **A10** (*m/z* 158), **A11** (*m/z* 60), **A12** (*m/z* 98), **A13** (*m/z* 126), **A14** (*m/z* 136). Then these small molecules underwent further mineralization into CO_2 and H_2O by the action of ROS.

The intermediates detected in the H_1S_2/PMS system varied from those observed in the P_1S_2-induced degradation of TC, further substantiating distinct degradation pathways. Utilizing the Fukui function and the characterized intermediates, Fig. 6e delineated plausible degradation pathways for TC [47,50]. It should be noted that in this system, free radicals and non-free radicals should work together. In hydroxylation pathway I, TC underwent initial oxidation mediated by $SO_4^{\bullet-}$/$^\bullet$OH and then hydroxyl groups were introduced into C40 and C38 sites, leading to the formation of ketone **B1** (*m/z* 478). As a result of additional oxidation of ROS, deamidation ensued, resulting in the formation of **B2** (*m/z* 378). Subsequently, as the degradation process progressed, **B2** underwent hydroxyl rearrangement and deamination, ultimately decomposing into **B3** (*m/z* 314). **B4** (*m/z* 249) was obtained through the loss of a carbon atom from a ring structure, hydroxylation at the C41 site, and then experienced demethylation and continuous oxidation, ultimately yielding **B5** (*m/z* 166). In pathway II, C38, C40, O24 sites were attacked firstly to generate **B6** (*m/z* 405) *via* hydroxyl groups connection and disruption of the cyclic hydrocarbon structure along with ring-opening process, following with deamidation to produce **B7** (*m/z* 310) and further transformed into **B8** (*m/z* 200) as well as **B9** (*m/z* 136) with oxidation by $SO_4^{\bullet-}$/$^\bullet$OH. The intermediates produced aforementioned underwent intense oxidation due to the persistent attack by ROS and decomposed by ring-opening reactions to **B10** (*m/z* 126), **B11** (*m/z* 114), **B12** (*m/z* 114), **B13** (*m/z* 112), **B14** (*m/z* 98), and **B15** (*m/z* 82). Ultimately, these compounds broke down further into H_2O, CO_2, and smaller organic molecules. Finally, the results of the toxicity assessment of the degradation

by-products by Toxicity Estimation Software Tool indicated the environmental friendliness of the catalytic system (Fig. S20 in Supporting information).

To sum up, by using different waste plastics as precursors, metal-free porous carbon catalytic materials with different characteristics were successfully synthesized under microwave carbonization. The as prepared carbon materials P_1S_2 and H_1S_2 exhibited excellent performance in TC removal; P_1S_2 achieved 100 % degradation with a rate constant of 0.303 min^{-1} in 20 min, while H_1S_2 reached the same degradation level with a rate constant of 0.235 min^{-1}. The carbon materials derived from waste plastics possessed outstanding practicability, which could accommodate different water environment substrates under a broad pH range (2.6–10.8) and the interference of various inorganic anions, while maintaining good recyclability. Mechanism studies showed that, in P_1S_2/PMS system, the TC degradation was mainly achieved through electron transfer nonradical pathway, with massive defects in P_1S_2 serving as the main active sites. Meanwhile, H_1S_2, which was rich in C–OH groups, achieved TC degradation through a radical process dominated by $SO_4^{\bullet-}$ and $^{\bullet}OH$. The different degradation pathways of TC were identified using LC-MS and Fukui function calculation, with the intermediates toxicity accurately predicted by T.E.S.T. This substantiated the effectiveness of the P_1S_2/PMS and H_1S_2/PMS systems in mitigating the eco-risks caused by antibiotic contaminants. This study not only embodied the concept of using waste to treat waste, but more importantly, it modulated the degradation mechanism of pollutants by adjusting different precursors of metal-free carbon materials.

Declaration of competing interests

The authors declare that they have no known competing financial interests or personal relationships that could have appeared to influence the work reported in this paper.

CRediT authorship contribution statement

Denghong Zhao: Methodology, Data curation, Writing – original draft, Project administration, Investigation. **Mingwei Yang:** Investigation. **Yichuan Zhang:** Investigation. **Long Qin:** Investigation. **Hang Liu:** Investigation. **Hongji Chen:** Investigation. **Maoguo Tan:** Investigation. **Zhongyi Yin:** Supervision. **Bin Sun:** Supervision. **Yu Shen:** Supervision, Funding acquisition. **Haijiao Xie:** Software. **Heyan Jiang:** Writing – review & editing, Funding acquisition, Project administration, Supervision, Conceptualization.

Acknowledgments

This work was financially supported by Natural Science Foundation Project of CQ (No. CSTB2023NSCQ-LZX0067), Science and Technology Research Program of Chongqing Municipal Education Commission (No. KJZD-K202200804), Venture & Innovation Support Program for Chongqing Overseas Returnees (No. cx2020113), National Natural Science Foundation of China (No. 21201184) and Chongqing Technology and Business University Graduate Innovative Research Project (No. CYS240548).

Supplementary materials

Supplementary material associated with this article can be found, in the online version, at doi:10.1016/j.cclet.2025.111631.

References

[1] W. Wang, X. Li, F. Deng, et al., Chin. Chem. Lett. 33 (2022) 5200–5207.
[2] Y. Hu, F.L. Meng, J.H. Zhao, et al., Water Res. 262 (2024) 122112.
[3] Y. Li, M. Fan, C. Wang, et al., Chin. Chem. Lett. 35 (2024) 109764.
[4] X. Mao, M. Wang, J. Li, et al., Appl. Catal. B: Environ. 331 (2023) 122698.
[5] L. Hu, Y. Zhang, X. Liu, et al., Chem. Eng. J. 450 (2022) 138219.
[6] R. Ji, J. Chen, T. Liu, X. Zhou, Y. Zhang, Chin. Chem. Lett. 33 (2022) 643–652.
[7] J. Xu, J. Song, Y. Min, Q. Xu, P. Shi, Chin. Chem. Lett. 33 (2022) 3113–3118.
[8] J. Xie, L. Zhang, X. Luo, et al., Chem. Eng. J. 457 (2023) 141149.
[9] H. Zhang, X. Gan, S. Chen, H. Yu, X. Quan, Sep. Purif. Technol. 292 (2022) 121048.
[10] M. Kohantorabi, G. Moussavi, S. Giannakis, et al., Chem. Eng. J. 411 (2021) 127957.
[11] X. Duan, Z. Ao, L. Zhou, et al., Appl. Catal. B: Environ. 188 (2016) 98–105.
[12] J. Wang, X. Duan, J. Gao, et al., Water Res. 185 (2020) 116244.
[13] J. Kang, X. Duan, L. Zhou, et al., Chem. Eng. J. 288 (2016) 399–405.
[14] J. Dou, J. Cheng, Z. Lu, et al., Appl. Catal. B: Environ. 301 (2022) 120832.
[15] F. Ye, Y. Su, R. Li, et al., Appl. Catal. B: Environ. 337 (2023) 122992.
[16] X. Duan, H. Sun, Y. Wang, J. Kang, S. Wang, ACS Catal. 5 (2015) 553–559.
[17] P. Wang, H. Zhang, Z. Wu, et al., Chin. Chem. Lett. 34 (2023) 108722.
[18] J. Mehta, N. Dilbaghi, A. Deep, et al., Carbon 234 (2024) 119969.
[19] A. Stubbins, K.L. Law, S.E. Muñoz, T.S. Bianchi, L. Zhu, Science 373 (2021) 51–55.
[20] Y. Luo, X. Lin, E. Lichtfouse, H. Jiang, C. Wang, Environ. Chem. Lett. 21 (2023) 3127–3158.
[21] W.A. Algozeeb, P.E. Savas, Z. Yuan, et al., ACS Nano 16 (2022) 7284–7290.
[22] X. Duan, H. Sun, S. Wang, Acc. Chem. Res. 51 (2018) 678–687.
[23] S. Ren, X. Xu, Z.S. Zhu, et al., Appl. Catal. B: Environ. 342 (2024) 123410.
[24] Q. Cao, X.F. Cheng, J. Wang, et al., Chin. Chem. Lett. 35 (2024) 108759.
[25] Q. Zhou, L. Qin, Z. Yin, H. Jiang, Sep. Purif. Technol. 328 (2024) 125033.
[26] H. Jiang, J. Zhou, Q. Zhou, et al., Chem. Eng. J. 489 (2024) 151256.
[27] C. Gan, Q. Zhou, M. Sheng, et al., J. Clean. Prod. 434 (2024) 140417.
[28] M. Sheng, C. Gan, Y. Li, et al., Appl. Catal. B: Environ. 339 (2023) 123138.
[29] N. Cai, X. Li, S. Xia, et al., Energy Convers. Manage. 229 (2021) 113794.
[30] T. Kan, V. Strezov, T.J. Evans, Renew. Sust. Energy Rev. 57 (2016) 1126–1140.
[31] H. Zhang, T. Tao, X. Li, et al., Int. J. Hydrogen Energy 45 (2020) 18057–18065.
[32] H. Yang, R. Qiu, Y. Tang, et al., Water Res. 231 (2023) 119659.
[33] X. Li, T. Han, Y. Zhou, et al., Appl. Catal. B: Environ. 350 (2024) 123913.
[34] S. Zhao, S.S. Shen, L. Han, B.C. Tian, N. Li, W. Chen, X.B. Li, Rare Met. 43 (2024) 4038–4055.
[35] Q. Zhou, L. Qin, H. Liu, et al., Chem. Eng. J. 487 (2024) 150370.
[36] C. Gan, M. Sheng, Z. Hu, et al., J. Catal. 413 (2022) 636–647.
[37] J.C.E. Yang, M.P. Zhu, D.D. Dionysiou, et al., Chem. Eng. J. 430 (2022) 133102.
[38] J. Wu, J. Wang, C. Liu, et al., Environ. Sci. Technol. 56 (2022) 13996–14007.
[39] W. Tian, H. Zhang, X. Duan, et al., ACS Appl. Mater. Interfaces 8 (2016) 7184–7193.
[40] H. Li, X. Zhang, S. Yang, Y. Sun, J. Qian, Environ. Sci. Technol. 58 (2024) 14005–14012.
[41] S. Ma, D. Yang, Y. Guan, et al., Appl. Catal. B: Environ. 316 (2022) 121594.
[42] F. Li, Z. Lu, T. Li, P. Zhang, C. Hu, Environ. Sci. Technol. 56 (2022) 8765–8775.
[43] Y. Wang, Y. Song, N. Li, et al., J. Hazard. Mater. 421 (2022) 126794.
[44] Y. Qi, B. Ge, Y. Zhang, et al., J. Hazard. Mater. 399 (2020) 123039.
[45] B. Zhou, L. Chen, F. Li, et al., Chin. Chem. Lett. 34 (2023) 108558.
[46] M. Zhang, J. Ruan, X. Wang, et al., Water Res. 246 (2023) 120697.
[47] Z. Xu, Y. Zhang, F. Wang, et al., Chem. Eng. J. 452 (2023) 139229.
[48] F. Wang, S.S. Liu, Z. Feng, et al., J. Hazard. Mater. 440 (2022) 129723.
[49] X. Li, S. Wang, P. Chen, et al., Appl. Catal. B: Environ. 325 (2023) 122401.
[50] F. Sun, X. Yang, F. Shao, et al., Chin. Chem. Lett. 34 (2023) 108563.